Available online at www.sciencedirect.com
ScienceDirect
Journal of Catalysis 248 (2007) 288–302
JOURNAL OF CATALYSIS
www.elsevier.com/locate/jcat

Influence of the preparative route on the properties of WO_x–ZrO_2 catalysts: A detailed structural, spectroscopic, and catalytic study

Agustín Martínez [a,*], Gonzalo Prieto [a], Maria A. Arribas [a], Patricia Concepción [a], Juan F. Sánchez-Royo [b]

[a] *Instituto de Tecnología Química, CSIC-UPV, Avda. de los Naranjos s/n, 46022 Valencia, Spain*
[b] *Departamento Física Aplicada y Electromagnetismo, ICMUV, Universidad de Valencia, Doctor Moliner 50, 46100 Burjassot, Spain*

Received 5 January 2007; revised 23 March 2007; accepted 24 March 2007

Abstract

Two series of tungstated zirconia (WZ) solid acids covering a wide range of tungsten surface densities (δ, W at/nm^2) were prepared by nonconventional impregnation and coprecipitation routes, leading to samples with enhanced surface area (∼70–120 m^2/g) on annealing at 973–1073 K. The materials were thoroughly characterized by N_2 physisorption, XRD, Raman, XPS, H_2-TPR, and DR UV–vis spectroscopy. The catalytic behavior of the Pt-promoted WZ catalysts (1 wt% Pt) was evaluated for the hydroconversion of *n*-hexadecane used as model feed representative of Fischer–Tropsch waxes. Both series of catalysts displayed a pronounced maximum in the reaction rate and a minimum in the selectivity to branched feed isomers (*iso*-C_{16}) at an intermediate tungsten density (δ_{max}). Interestingly, we found that δ_{max} shifted toward higher values for coprecipitated catalysts ($\delta_{max,COP} = 6.8$ W at/nm^2) compared with the impregnated ones ($\delta_{max,IMP} = 5.2$ W at/nm^2). This has been ascribed to a better inherent capacity of the coprecipitation route for dispersing tungsten species on the ZrO_2 surface, as inferred from modeled XPS data. This determines that both the formation of highly interconnected amorphous WO_x domains required for the generation of catalytically active Brønsted acid sites and the onset of growth of inactive three-dimensional WO_3 crystallites (ascertained by XRD and Raman) occur at higher tungsten surface densities in WZ solids generated by coprecipitation than in those obtained by impregnation. Despite the observed shift in δ_{max}, the two most active samples within each series displayed nearly the same intrinsic activity per total W atoms, suggesting that a similar nature and size for the supported active WO_x domains should be attained by both impregnation and coprecipitation routes at $\delta = \delta_{max}$. Moreover, the method of preparation was found to affect the optical and electronic properties of the supported WO_x species. Thus, coprecipitation provides WZ solids displaying a lower valence–conduction energy gap, as well as enhanced reducibility for the polytungstate domains due to an improved electronical linkage with the zirconia support, in opposition to a more isolated character of the WO_x clusters generated by impregnation.

Keywords: Tungstated zirconia; Impregnation; Coprecipitation; Tungsten surface density; Pt-promoted WZ catalysts; Hydroconversion of *n*-hexadecane; Fischer–Tropsch waxes; XRD; Raman; XPS; UV–vis spectroscopy

1. Introduction

Tunsgtated zirconia materials are very attractive, environmentally friendly solid acids. When promoted by noble metals (e.g., Pt) and in the presence of H_2, these materials display high catalytic activity and stability in demanding reactions requiring strong Brønsted acidity, such as the skeletal isomerization of short-chain linear alkanes [1–7]. These catalysts also show good isomerization selectivities during the hydroconversion of long-chain *n*-alkanes [8–12], a key process in the production of ultra-clean diesel fuels from Fischer–Tropsch waxes [13,14]. Although less active than their sulfate-promoted counterparts, tungstated zirconia catalysts offer inherent advantages over the former from the standpoint of industrial application, such as higher stability under high-temperature treatments and reductive atmospheres, lower deactivation rates during catalysis, and easier regeneration [5,15–17].

* Corresponding author. Fax: +34 963 877 809.
E-mail address: amart@itq.upv.es (A. Martínez).

0021-9517/$ – see front matter
doi:10.1016/j.jcat.2007.03.022

A minimum level of WO_x doping is required to completely stabilize the tetragonal phase of the zirconia support on annealing in air at the high temperatures (typically 973–1173 K) needed to produce catalytically active materials [18]. Interestingly, Iglesia and co-workers reported that the acid activity of WO_x–ZrO_2 materials (abbreviated as WZ) is a unique function of the tungsten surface density (δ, given as W at/nm^2), rather than the W loading or calcination temperature independently [6,19]. When this parameter is considered, a maximum in the catalyst activity is generally found at intermediate values of the tungsten density, corresponding to a surface coverage around or slightly exceeding the theoretical monolayer [6,19]. Structural characterization of WZ materials using different spectroscopic techniques, such as Raman [20–22], UV–vis [6,23,24], and EXAFS [21,23], revealed that interconnecting two-dimensional polyoxotungstates are the prevailing species at coverages around the monolayer, where the maximum activity is attained. It has been proposed that strong Brønsted acid sites responsible for the high catalytic activity of WZ develop on reduction of W^{6+} species in the presence of H_2 or other reductants, such as alkanes and alcohols, to compensate for the excess negative charge in the polyoxotungstate domains [24–26]. These types of active sites are termed *temporary* acid sites, in opposition to the *permanent* acidity present in calcined WZ samples. By themselves, the last kind of acid sites cannot account for the observed catalytic activity [22,24]. At tungsten coverages well below the monolayer, isolated monotungstate species predominate on the zirconia surface [21,27]. These species are difficult to reduce and thus do not allow for the formation of catalytically active Brønsted acid sites. In contrast, highly reducible three-dimensional WO_3 crystallites coexist with the two-dimensional amorphous polytungstates at coverages exceeding the monolayer, resulting in decreased accessibility to the active WO_x species. Thus, the occurrence of a maximum in the catalytic activity at intermediate WO_x surface densities represents a compromise between the accessibility to the surface WO_x species and their reducibility [5,6,28].

Whereas it appears that the structural, acidic, and catalytic properties of WZ samples (and their Pt-promoted versions) can be well rationalized on the basis of the tungsten surface density (δ), at least for homogeneous series of catalysts prepared by the same procedure, the picture is not so clear when dealing with samples prepared by different routes. Thus, significant divergences are found in the literature when comparing samples obtained by, for instance, impregnation of hydrous zirconia with tungstate and by coprecipitation or sol–gel methods. In this respect, Falco et al. [29] reported substantial differences in conversion during the hydroisomerization of *n*-hexane on Pt/WZ samples prepared by different methods. These authors did not find a clear correlation between the catalytic activity and catalyst properties such as surface area, mean pore diameter, percentage of tetragonal ZrO_2 phase, acidity, and presence of WO_3 crystallites [29], although no attempt was made to correlate the activity with the tungsten surface density (δ) of the samples. However, we completed the exercise from the data reported in the paper and found significant differences in activity for the various methods used when compared at similar values of δ. In a previous study, Santiesteban et al. [30,31] found that a WZ sample prepared by coprecipitation contained twice the amount of strong acid sites and displayed higher activity for *n*-pentane isomerization compared with another one obtained by impregnation, both with similar W loadings and surface areas and thus similar tungsten surface density. The X-ray diffractograms reported in that work clearly revealed that the intensity of the peaks associated with three-dimensional WO_3 crystallites was much higher for the impregnated catalyst, suggesting that the coprecipitation method favored the dispersion of the WO_x species on the zirconia surface retarding the formation of WO_3 crystallites. Other authors also emphasized the high degree of dispersion of WO_x species achieved in WZ materials prepared by coprecipitation [32] and sol–gel routes [33]. Moreover, Boyse and Ko [18] studied the behavior of samples prepared by impregnation and sol–gel methods as a function of the oxidation temperature, and found that at constant W loading, the samples obtained by one-step sol–gel synthesis required higher oxidation temperatures to become active for the skeletal isomerization of *n*-butane. This was due to the fact that in sol–gel samples tungsten species must first be expelled from the bulk before they form the active WO_x species on the zirconia surface. Using infrared (IR) spectroscopy, these authors concluded that the active WO_x species were the same regardless of the preparation method used [18].

It follows from the above discussion that further work is needed to better understand the influence of the preparative route on the physicochemical and catalytic properties of WZ (and Pt/WZ) materials. For this purpose, in this work we prepared two series of WZ samples covering a wide range of δ by using impregnation and template-assisted coprecipitation procedures leading to samples with both high and comparable specific surface areas. The materials have been thoroughly characterized by XRD, N_2 physisorption, H_2-TPR, diffuse reflectance UV–vis spectroscopy, Raman, and XPS. We studied the catalytic behavior of the Pt-promoted samples for the hydroconversion of *n*-hexadecane, which we used as model feed representative for the long-chain *n*-paraffins contained in Fischer–Tropsch waxes.

2. Experimental

2.1. Catalyst preparation

Two series of WZ samples with different tungsten surface densities (δ) were prepared by impregnation and coprecipitation methods as follows.

2.1.1. Impregnation

First, zirconium oxohydroxide, $ZrO_x(OH)_{4-2x}$, was precipitated by drop wise addition of a 0.53 M aqueous solution of $ZrOCl_2$ (Aldrich, 98% $ZrOCl_2{\cdot}8H_2O$) to a NH_4OH (2 M)/NH_4Cl (2 M) buffer solution to keep the pH at a constant value of 10.5 during the precipitation. Previous studies showed that precipitation at high pH values produced $ZrO_x(OH)_{4-2x}$ with increased surface area and pore volume [6,34]. After hydrolysis, the solid was filtered and exhaustively washed with

distilled water until the absence of chlorides. The wet precipitate was suspended in a basic aqueous solution (pH 10.5) and aged overnight at reflux conditions. After aging, the sample was filtered, washed, and finally dried at 333 K overnight. The dried solid was impregnated with an excess (3 cm^3/g) of an aqueous solution containing the required amount of ammonium metatungstate [$(NH_4)_6H_2W_{12}O_{40}$, Fluka, >85% WO_3] to obtain different W loadings in the range 12–23 wt%, followed by evaporation of the water solvent in a rotary evaporator. Then the impregnated materials were dried at 333 K overnight and finally calcined under air flow at either 973 or 1073 K for 3 h to produce solids with tungsten surface densities ranging from 3.3 to 7.3 W at/nm^2.

2.1.2. Template-assisted coprecipitation

This series of samples was prepared by coprecipitation of the zirconium and tungsten precursors in the presence of polyvinyl alcohol (PVA) as reported previously [35] with some modifications. In brief, 300 cm^3 of a zirconyl chloride (0.53 M) and ammonium metatungstate (required amount for desired loading) aqueous solution was heated at 373 K in an oil bath and kept at this temperature for 1 h. In parallel, 300 cm^3 of PVA ($M_w = 7 \times 10^4$–9×10^4, Sigma) aqueous solution (100 g/L) was heated at 373 K in an oil bath for 1 h. Then the two solutions were mixed and kept at 373 K for an additional hour. The mixed solution was cooled until 343 K, slowly added to a NH_4OH (2 M)/NH_4Cl (2 M) buffer solution, and kept for 1 h in static. Then the formed transparent gel filaments were extensively washed with distilled water until the absence of chlorides and dried at 373 K overnight and at 473 K for an additional 12 h. Thereafter, the solid was carbonized under nitrogen flow at 673 K for 2 h and then at 973 K for 2 h. Finally, the polymer template was removed by calcination under air flow at 773 K for 5 h, after which the temperature was raised to the desired annealing temperature (1073 K) and kept there for 3 h. A heating rate of 2 K/min was used in all of these thermal treatments. The presence of the PVA polymer during the synthesis was shown to produce materials with higher surface areas than those prepared by conventional coprecipitation [35]. The W loading was varied from 6 to 22 wt%, producing samples with tungsten densities from 4.5 to 9.9 W atoms/nm^2 after annealing at 1073 K.

The prepared samples were denoted by WZ(M, δ), where M refers to the preparation method (M = I for impregnation and C for coprecipitation) and δ is the tungsten surface density in W at/nm^2.

Pt-promoted WZ catalysts were prepared by incipient wetness impregnation of the WZ samples with a 0.2 N HCl aqueous solution containing the required amount of hexachloroplatinic acid (H_2PtCl_6, Sigma) to obtain a nominal Pt concentration of 1 wt% in the final catalysts. After impregnation, the samples were dried at 373 K overnight, then calcined in air flow at 773 K for 3 h.

A bulk monoclinic WO_3 sample was also prepared by calcining ammonium metatungstate in a muffle oven at 873 K for 6 h. This sample is used as reference when discussing some of the characterization results reported in this work.

2.2. Characterization techniques

The tungsten content in the WZ samples was determined by ICP. Powder X-ray diffraction (XRD) patterns were recorded in a Philips PW 1830 apparatus using Ni-filtered Cu$K\alpha$ radiation. XRD was used to quantify the relative amounts of tetragonal and monoclinic ZrO_2 phases in the calcined WZ samples and to detect the presence of bulk WO_3 crystallites. BET surface areas were determined by N_2 adsorption at 77 K on a Micromeritics ASAP-2000 instrument after sample pretreatment at 673 K and vacuum overnight.

Raman spectra were acquired with a Renishaw Raman In Via spectrometer equipped with a Leika DM LM microscope and a 785-nm HPNIR diode laser as an excitation source. The laser power at the sample was 30 mW. A 50× objective of 8 mm optical length was used to focus the depolarized laser beam onto a 3–5 μm spot on the sample surface and collect the backscattered light. The Raman scattering was collected in a static-scan mode in the 100–3000 cm^{-1} spectral region with a resolution >4 cm^{-1}. Ten scans were accumulated for each spectrum for a total scanning time of 100 s.

X-ray photoelectron spectra were recorded on a VG Escalab 210 spectrophotometer using Al$K\alpha$ radiation (1486.6 eV) at 15 kV and 20 mA, and operating in a constant pass energy mode (20 eV pass energy). The samples were grounded, pressed into a small disc, and evacuated in the prechamber of the spectrometer at 1.3×10^{-7} Pa. The following regions were recorded: O 1s, Zr 3d, W 4f, Zr 4p, and C 1s. All core electron binding energies (BEs) were referenced to the Zr $3d_{5/2}$ peak at 182.5 eV. The measured intensity ratios of components were obtained from the area of the corresponding peaks after nonlinear Shirley-type background subtraction.

Hydrogen temperature-programmed reduction (H_2-TPR) was performed in a Micromeritics Autochem 2910 equipment. A ca. 100-mg Pt-loaded sample was first flushed with 30 cm^3/min of Ar at room temperature (RT) for 30 min, after which a mixture of 10 vol% of H_2 in Ar was passed through the solids at a flow rate of 50 cm^3/min. Then the temperature was increased up to 1173 K at a heating rate of 10 K/min. The H_2 consumption was monitored in a thermal conductivity detector (TCD) that had been calibrated using the reduction of CuO as a standard.

Diffuse reflectance UV–vis (DR UV–vis) spectra were collected on a Cary 5 apparatus equipped with a "Praying Mantis" attachment from Harrick. The sample cell was equipped with a reaction chamber, thus enabling in situ treatments. $BaSO_4$ was used as reflectance standard at the measurement temperatures. In a set of experiments, the oxidized WZ samples were degassed at 423 K in flowing Ar for 2 h before the spectra were recorded. Another set of experiments involved in situ reduction treatments in both Pt-loaded and Pt-free WZ samples. Typically, ca. 130 mg of sample were first dehydrated in flowing Ar as before, and then the gas was switched to H_2 and the temperature was increased to 523 K and maintained at this value for 2 h before recording the spectra under flowing H_2. To determine the kinetics of the reduction process, the spectra were recorded every 15 min during the first hour

and then every 30 min thereafter until a stationary state was reached.

2.3. n-Hexadecane hydroconversion experiments

The hydroconversion of *n*-hexadecane (Sigma, 99%) was carried out in a continuous-downflow fixed-bed reactor at a total pressure of 4.0 MPa, $H_2/n\text{-}C_{16}$ molar ratio of 95, and space velocity (WHSV) of 3.6 h^{-1}. Typically, the reactor was loaded with 1.0 g of catalyst with a particle size of 0.2–0.4 mm diluted with SiC (0.6–0.8 mm particle size) to a constant volume of 5.5 cm^3. Before starting the catalytic experiments, Pt/WZ catalysts were reduced in situ by passing a flow of pure H_2 (300 cm^3/min) through the reactor at atmospheric pressure and 523 K for 2 h. After the reduction was completed, the temperature was set to the desired reaction temperature, the total pressure was increased to 4.0 MPa, and the H_2 and $n\text{-}C_{16}$ flow rates were adjusted to attain a $H_2/n\text{-}C_{16}$ ratio of 95. Pure *n*-hexadecane was fed by means of a high-precision HPLC pump (Gilson 305) at the flow rate of 3.6 g/h. The stream leaving the reactor was depressurized and analyzed online in a Varian Star 3800 CX gas chromatograph equipped with a capillary column (Petrocol DH 50.2TM, 50 m × 0.2 mm, 0.5 μm film, Supelco) and a flame ionization detector (FID). To avoid any condensation of the heaviest hydrocarbons, all transfer lines from the reactor to the gas chromatograph were carefully heated to 548 K while diluting the product stream with a flow of nitrogen. The reactor conditions were maintained until a nearly constant composition of the reaction products (pseudostationary state) was observed before setting the reactor temperature to a new value. At the end of the experiment, the initial reaction conditions were reestablished to verify the absence of significant catalyst deactivation. All the catalytic data given in this work correspond to those obtained in the pseudostationary state, which was typically attained after about 2 h on stream.

3. Results and discussion

3.1. Chemical composition and BET surface area of WZ samples

The tungsten content, BET surface area, and tungsten surface density (δ) of WZ samples prepared by the impregnation and PVA-assisted coprecipitation methods are given in Table 1. As mentioned earlier, the samples obtained by the two methods used here displayed larger surface areas than those prepared by conventional impregnation and coprecipitation procedures. Moreover, both methods led to solids with comparable BET values at similar W content when calcined at the same temperature. Thus, it appears that the initial presence of the tungsten species on the surface in the impregnated samples and in the bulk in the coprecipitated ones does not significantly alter the surface area of the final solids. In the present work, different values of δ were obtained in the impregnated series by varying both the W loading (12–23 wt%) and oxidation temperature (973 and 1073 K). In the samples prepared by the PVA-templated coprecipitation route, δ was varied by changing the W loading (6–22 wt%) while maintaining a constant oxidation temperature of 1073 K to ensure complete migration of the tungsten species from the bulk of the mixed W–Zr solid to the surface of zirconia.

Table 1
BET surface area and chemical composition of oxidized WZ samples prepared by impregnation and PVA-assisted coprecipitation

Sample	W content (wt%)	T_{calc} (K)	BET (m^2/g)	δ[a] (W at/nm^2)
WZ(I,3.3)	12	973	120	3.3
WZ(I,3.9)	15	973	126	3.9
WZ(I,4.7)	13	1073	90	4.7
WZ(I,5.2)	19	973	120	5.2
WZ(I,5.5)	14	1073	83	5.5
WZ(I,5.9)	15	1073	83	5.9
WZ(I,6.1)	21	973	113	6.1
WZ(I,7.3)	23	973	103	7.3
WZ(C,4.5)	6	1073	44	4.5
WZ(C,5.5)	15	1073	89	5.5
WZ(C,6.8)	18	1073	87	6.8
WZ(C,7.3)	19	1073	85	7.3
WZ(C,9.9)	22	1073	73	9.9

[a] Tungsten surface density.

3.2. Hydroconversion of n-hexadecane on Pt/WZ catalysts

The hydroisomerization of *n*-alkanes on Pt/zeolite catalysts proceeds through the classical bifunctional metal–acid mechanism first proposed by Weisz [36]. According to this mechanism, the *n*-alkane reactant molecule is first dehydrogenated on the metal site (e.g., Pt), followed by protonation of the intermediate *n*-alkene and subsequent rearrangement (isomerization) of the adsorbed carbocation on a Brønsted acid site of the zeolite. In the last step of the mechanism, the branched alkene desorbed from the acid site is hydrogenated on a metallic center to give the final branched alkane. On a well-balanced catalyst, rearrangement of the carbocations on the Brønsted acid sites is the rate-determining step, and thus, in the absence of steric constraints, the isomerization rate is governed by the zeolite acidity. Whereas some authors have proposed that this classical bifunctional mechanism is also operative in the case of Pt/WZ catalysts during the isomerization of short-chain *n*-alkanes [7,37,38], others have suggested a nonclassical bifunctional mechanism in which the initial activation of the *n*-alkane molecules occurs in a redox step involving partially reduced tungsten species [39–41]. In this case, the main role of the Pt^0 centers is to supply dissociated hydrogen necessary for the generation of Brønsted acid sites on the partially reduced WO_x domains, and for rapid desorption of the adsorbed carbocations avoiding extensive cracking and coking reactions. Although the participation of the classical bifunctional mechanism cannot be completely ruled out, it cannot account for the high isomerization activity displayed by Pt/WZ catalysts at reaction temperatures where Pt/zeolites are almost inactive [3,12] if, as supported by experimental data, the strength of the Brønsted acid sites in Pt/WZ materials is not higher than those in zeolites and thus far below the *superacidity* range

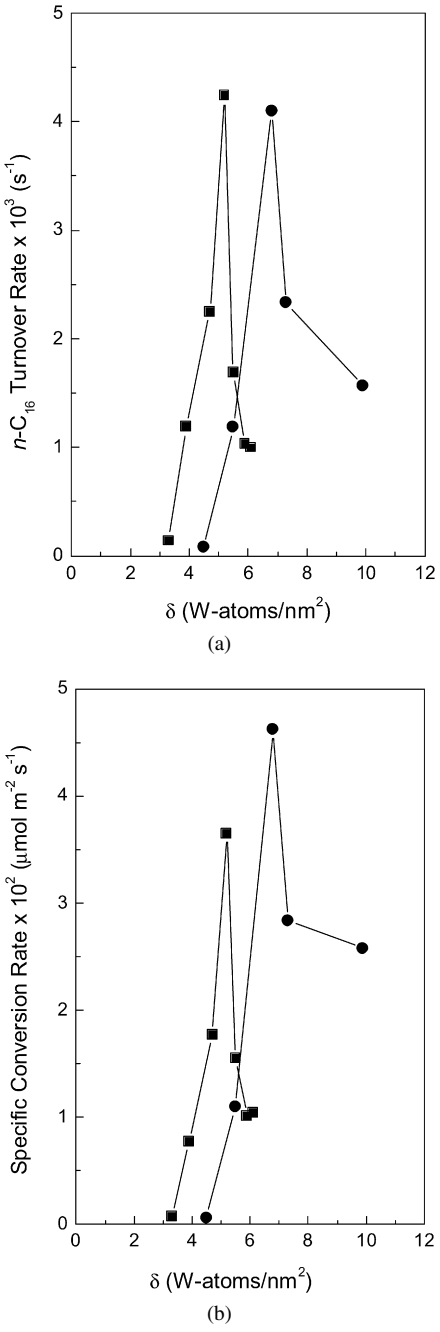

Fig. 1. Catalytic activity for the hydroconversion of *n*-hexadecane of Pt/WZ catalysts prepared by impregnation (■) and coprecipitation (●) as a function of tungsten surface density (δ): (a) Turnover rate (in moles of n-C_{16} converted per total moles of W and second), and (b) Specific reaction rate (in μmol converted per m^2 and second). Reaction conditions: $P = 4.0$ MPa, H_2/hydrocarbon molar ratio of 95, WHSV $= 3.6\ h^{-1}$ (the conversion was varied by changing temperature).

[12,25,42–44]. The predominance of the proposed nonclassical bifunctional mechanism is also supported by the effect of Pt on the isomerization activity of Pt/WZ catalysts. In contrast to what is known for Pt/zeolite catalysts, it seems from the results reported in the literature that only a few accessible Pt^0 centers are required to promote the isomerization activity in Pt/WZ materials [45,46]. In fact, Falco et al. [29] concluded that the formation of dissociated hydrogen is not a limiting factor for Pt/WZ catalysts at Pt concentrations above 0.05 wt%, and thus, the reaction is controlled mainly by the acidic properties of the WZ support. Taking this into account, together with the relatively high Pt loading (1 wt%) and metal dispersions obtained for our samples [12], we can conclude that the changes in activity and selectivity observed during the hydroconversion of *n*-hexadecane when varying the W surface density and method of preparation of Pt/WZ samples, as discussed below, are related to differences in the acidic properties of the materials.

Fig. 1a presents the change of the turnover rate (molecules of n-C_{16} converted per W atom per second) at a reaction temperature of 453 K with the tungsten surface density (δ) for the series of Pt/WZ catalysts obtained by impregnation and PVA-assisted coprecipitation. The same qualitative behavior is observed for both series; that is, the turnover rate passes through a sharp maximum at an intermediate value of δ, hereinafter generally denoted as δ_{max}, and particularly $\delta_{max,IMP}$ or $\delta_{max,COP}$ when referring to the W density of maximum catalytic activity in the impregnated or coprecipitated series, respectively. This general trend concurs with previous observations on samples prepared by impregnation [6,7,19] and, as reported here, appears to be independent of the method of preparation. In previous work, Iglesia et al. [6] found that the turnover rate for the acid-catalyzed isomerization of *o*-xylene on WZ samples prepared by a similar impregnation method to that used here depended only on the tungsten surface density (δ) over a wide range of W contents (5–21 wt%) and oxidation temperatures (773–1223 K). The results obtained in the present work confirm that this finding is also valid for the hydroconversion of *n*-hexadecane. In fact, Fig. 1 clearly shows that nearly the same activity is obtained for impregnated samples Pt/WZ(I,5.9) and Pt/WZ(I,6.1) having almost the same W surface density but calcined at 1073 and 973 K, respectively.

Although both series of catalysts display the same general trend in activity with δ, the results in Fig. 1a reveal clear differences between the two preparation methods. First, δ_{max} is shifted toward higher values in the coprecipitated samples (6.8 vs 5.2 W at/nm^2 for the impregnated catalysts), and second, the decrease in the turnover rate at W surface densities above δ_{max} is much more drastic in the impregnated series. It is clear from these results that we must be very cautious when comparing WZ samples prepared by different methods, because quite distinct conclusions will be obtained depending on the δ value at which the comparison is done. In this respect, it is not surprising in light of our results that Santiesteban et al. found that a WZ sample prepared by coprecipitation with $\delta = 8.2$ W at/nm^2 was significantly more acidic and catalytically active than another WZ sample obtained by impregnation and having a similar tungsten surface density ($\delta = 8.9$ W at/nm^2) [30]. However, the opposite conclusion might be reached if the samples are compared at δ values <6 W at/nm^2, as clearly deduced from the results presented in Fig. 1a. Furthermore, it should be noted that a similar TOF is obtained for the most active WZ(I,5.2) and WZ(C,6.8) catalysts, implying that equally active catalysts can be prepared by impregnation and coprecipitation provided that the optimum tungsten surface density (δ_{max}) is attained in

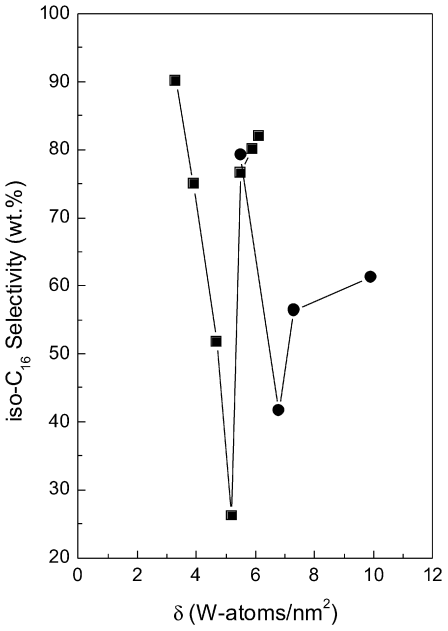

Fig. 2. Selectivity to isohexadecanes at 60% conversion for Pt/WZ catalysts prepared by impregnation (■) and coprecipitation (●) as a function of tungsten surface density (δ). Reaction conditions as indicated in Fig. 1.

each case. Nevertheless, comparing the catalytic activities of the two samples with $\delta = \delta_{max}$ within each series on the basis of specific reaction rates (per unit surface area) reveals that the sample prepared by coprecipitation is more active than that obtained by impregnation (Fig. 1b). Later in the article, we give a plausible explanation for this effect, in light of some of the characterization data reported in this work.

In recent work, we showed that at constant conversion, the most active catalyst of the coprecipitated series ($\delta = 6.8$ W atoms/nm^2) was that giving the lowest selectivity to hexadecane isomers (*iso*-C_{16}) or, equivalently, the highest selectivity to hydrocracked (C_3–C_{13}) products [12]. Here we complete the picture by plotting the *iso*-C_{16} selectivity at a constant *n*-C_{16} conversion of 60% as a function of δ for the two series of Pt/WZ samples (Fig. 2). As shown in this figure, the isomerization selectivity follows a well-defined pattern with increasing δ irrespective of the method of preparation used; that is, the selectivity to isohexadecanes first decreases with δ, reaches its minimum for the most active sample within each series (i.e., at $\delta = \delta_{max}$), and then increases again at $\delta > \delta_{max}$. Although both series of catalysts display the same general trend in selectivity, some differences are seen, as already noted when discussing the activity; that is, the selectivity curve is shifted toward higher values of δ, and the change in *iso*-C_{16} selectivity beyond δ_{max} is less pronounced in the coprecipitated series.

The occurrence of a maximum in the catalytic activity of WZ solids (and their Pt-promoted versions) at intermediate tungsten surface densities, corresponding to coverages around or slightly exceeding the theoretical monolayer of WO_x species on the ZrO_2 surface, also has been reported by others [6,7,18]. The increased activity when approaching the theoretical monolayer coverage has been related to an increase in the domain size of the partially reduced WO_x clusters and thus to their ability to delocalize the negative charge required for the generation of catalytically active Brønsted acid sites [6]. On the basis of low-temperature FTIR of adsorbed CO, Vu et al. [25] reported a maximum in the amount of Brønsted acid sites specific to the amorphous polytungstate domains at a W coverage around the theoretical monolayer. Moreover, by DRIFTS of adsorbed CD_3CN in prereduced Pt/WZ samples, we observed the presence of Brønsted acid sites of a lower strength at coverages below the monolayer [12], whereas at coverages above the monolayer, three-dimensional WO_3 crystallites start to develop on the zirconia surface, leading to decreased accessibility to the strong Brønsted acid sites [6,19,47]. These changes in the density and strength of the Brønsted acid sites with the tungsten coverage account not only for the maximum in activity, but also for the minimum in *iso*-C_{16} selectivity observed at intermediate W surface densities ($\delta = \delta_{max}$). In fact, increasing both the density and strength of the Brønsted acid sites (i.e., when approaching δ_{max}) is expected to decrease the selectivity to *iso*-C_{16} in favor of cracked products (i.e., hydrocarbons with fewer than 16 carbon atoms). In the first case, a higher density of acid sites will increase the probability of cracking of *iso*-C_{16} when diffusing out of the catalyst pores; in the second case, a higher acid strength will enhance the average lifetime of the adsorbed *iso*-C_{16}^+ cations and thus the probability of undergoing cracking into lighter products.

An exhaustive characterization study was undertaken to gain more insight into the observed divergences in the δ-dependence for the activity and selectivity of Pt/WZ catalysts prepared by impregnation and coprecipitation routes. The results are discussed in the following sections.

3.3. Structural properties of oxidized WZ samples

The presence of zirconia and tungsten oxide crystalline phases in oxidized WZ samples was ascertained by XRD. The X-ray diffractograms of the solids prepared by impregnation and coprecipitation are shown in Fig. 3. Complete stabilization of the tetragonal ZrO_2 phase was achieved in the impregnated samples after oxidation at 973–1073 K in the entire range of tungsten surface densities studied (Fig. 3a). This was also the case for the coprecipitated samples annealed at 1073 K (Fig. 3b) except the sample with the lowest tungsten density, WZ(C,4.5), which comprises a mixture of ca. 77% of tetragonal and 23% monoclinic ZrO_2, as estimated from the intensities of the (1 1 1) and (1 1 −1) reflections of the tetragonal and monoclinic phases, respectively [48]. This suggests that the amount of tungsten species interacting with zirconia in the coprecipitated W–Zr solid was not high enough to inhibit the partial crystallization into the thermodynamically stable monoclinic phase during the oxidation treatment.

The formation of bulk WO_3 crystallites also can be followed by XRD. Previous studies showed that monoclinic WO_3 microcrystallites (identified by the reflections in the 2θ range of 23°–25°) developed on the zirconia surface at tungsten coverages above the monolayer as a result of the agglomeration of surface WO_x species [12,18,28]. As shown in Fig. 3, the tungsten surface density at which this species starts to become

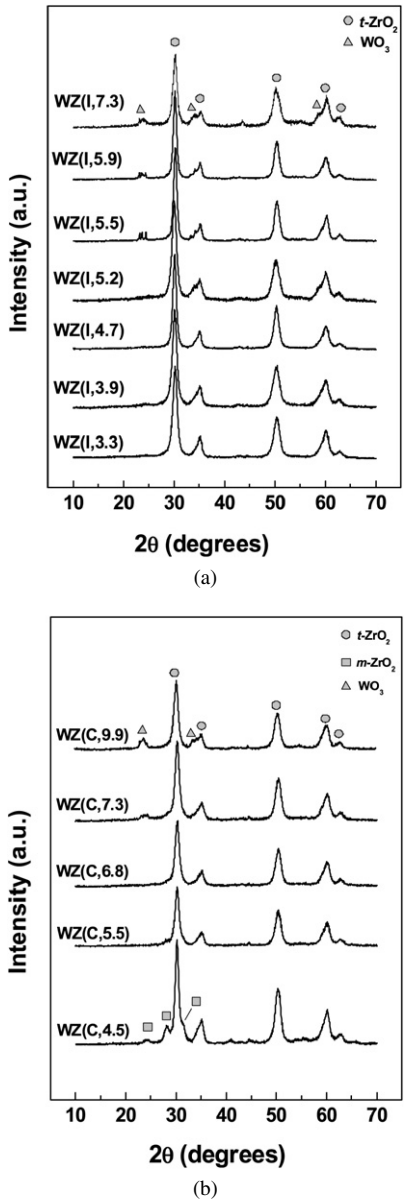

Fig. 3. X-ray diffraction patterns of oxidized WZ samples prepared by (a) impregnation and (b) coprecipitation methods.

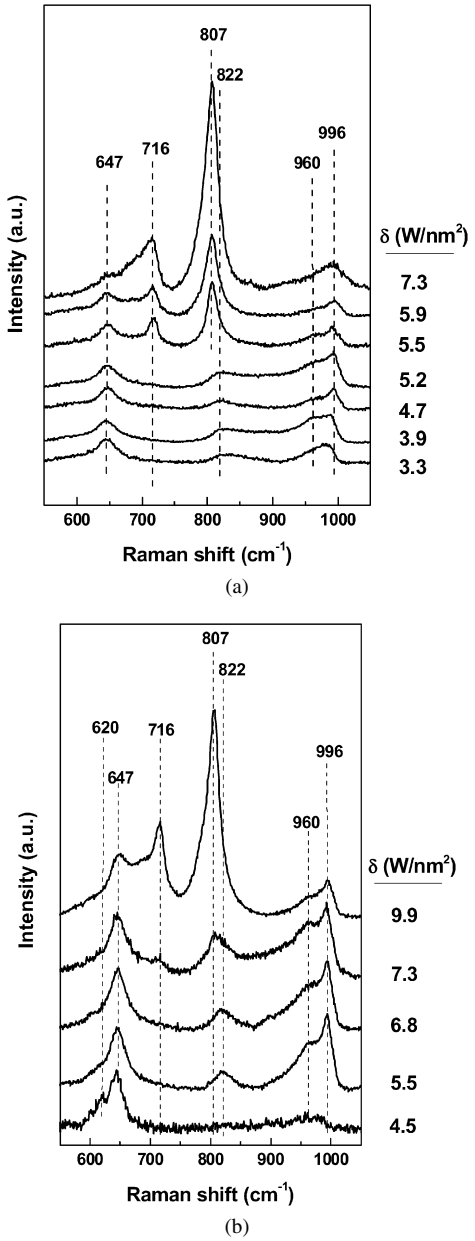

Fig. 4. Laser Raman spectra of oxidized WZ samples prepared by (a) impregnation and (b) coprecipitation methods.

clearly visible by XRD differs for the two preparation methods: 5.5 W at/nm^2 for the impregnated series and 7.3 W at/nm^2 for the coprecipitated series. This suggests that the coprecipitation method favors a high dispersion of the WO_x species segregated from the bulk of the mixed W–Zr oxyhydroxide to the zirconia surface during oxidation, thus retarding the appearance of the bulk WO_3 phase up to W surface densities higher than in the impregnated samples. A high dispersion of the WO_x species on the surface of ZrO_2 in solids prepared by coprecipitation and sol–gel methods also has been reported by others [32,33].

On the other hand, Raman spectroscopy is a very sensitive technique for detecting the presence of very small WO_3 crystallites [49]. The Raman spectra taken at ambient temperature for oxidized WZ samples prepared by impregnation and coprecipitation with different tungsten densities are given in Fig. 4. All samples display in the lower-frequency region the band at ca. 647 cm^{-1} characteristic of tetragonal zirconia. In addition, a band at ca. 620 cm^{-1} of monoclinic zirconia is seen in the sample prepared by coprecipitation with the lowest W surface density (4.5 W at/nm^2). These features related to the zirconia support are in agreement with the XRD data discussed above. The bands corresponding to surface tungsten species are observed at higher Raman shifts. For both the impregnated and coprecipitated series, the only tungsten bands observed at $\delta \leqslant \delta_{max}$ are those at 822 cm^{-1} assigned to W–O–W stretching modes and at 960 and 996 cm^{-1} attributed to W=O vibrations in hydrated interconnecting polyoxotungstate clusters [24]. These WO_x species generally have been associated with the formation of strong Brønsted acid sites under a reducing environment [39]. At tungsten surface densities above δ_{max},

Table 2
Bulk and surface W/Zr atomic ratios for WZ samples prepared by impregnation and coprecipitation, and corresponding values for the two parameters (c, θ) derived from the XPS model applied

Sample	W/Zr atomic ratio		XPS model parameters	
	Bulk[a]	Surface	c (nm)	θ
WZ(I,3.9)	0.12	0.21	0.37	0.46
WZ(I,4.7)	0.10	0.17	0.28	0.72
WZ(I,5.2)	0.17	0.23	0.32	0.69
WZ(I,5.5)	0.11	0.19	0.32	0.76
WZ(I,5.9)	0.12	0.22	0.37	0.68
WZ(I,7.3)	0.22	0.25	0.40	0.78
WZ(C,5.5)	0.12	0.25	0.43	0.56
WZ(C,6.8)	0.16	0.23	0.37	0.78
WZ(C,7.3)	0.17	0.20	0.33	0.95
WZ(C,9.9)	0.20	0.27	0.43	0.98

[a] Assuming tungsten in the form of WO_3.

two new bands at about 716 and 807 cm^{-1}, associated with W=O bending and stretching modes, respectively, in microcrystalline WO_3 species [50,51], are seen for the two series of samples. Thus, the Raman results confirm what was previously observed by XRD—that the onset of development of WO_3 crystallites occurs at tungsten surface densities of 5.5 W at/nm^2 for the impregnated sample and 7.3 W at/nm^2 for the coprecipitated sample. Interestingly, those values correspond to the W densities for which the catalytic activity started to decline in each series (Fig. 1). It appears, however, that the growth of three-dimensional WO_3 species after surpassing δ_{max} is favored in the impregnated series, for which quite intense WO_3 bands are already observed at $\delta = 5.5$ W at/nm^2, whereas the intensity of these bands is still modest for the coprecipitated sample with $\delta = 7.3$ W at/nm^2. Moreover, the slower rate of growth of WO_3 crystallites on the ZrO_2 surface observed for the coprecipitated samples concurs with the less drastic changes in activity and selectivity observed in this series at $\delta > \delta_{max}$.

XPS characterization was used to study the surface composition of the WZ samples as a function of δ and the method of preparation. The bulk and surface W/Zr atomic ratios, obtained by ICP and XPS analysis, respectively, are given in Table 2. Surface W/Zr atomic ratios were obtained by applying the Wagner sensitivity values to the XPS intensity values [52]. Tungsten surface enrichment is observed for both the impregnated and coprecipitated samples. Moreover, comparable surface W/Zr atomic ratios are obtained for the two series, indicating that the activation treatment at 1073 K was effective in expelling tungsten from the bulk to the surface of the coprecipitated WZ solid, validating the comparison in this work of samples prepared by the two methods in terms of the W surface density (δ) parameter.

Theoretical models have been applied to the XPS intensity values to try to correlate the tungsten spreading on the catalyst surface with the method of preparation and the tungsten surface density (δ). Thus, the Kerkhof and Moulijn (KM) model has been widely used in XPS for quantitative analysis of catalysts [53–55]. This model is well applied for high-surface area materials (finite support thickness) in which the catalyst is represented as a series of slabs supporting cubic dispersed-phase particles [56]. Due to the relatively low surface area of WZ materials (<130 m^2/g), the KM model cannot be successfully applied in the present study; instead, a more general model must be used taking into account the basic dependence for the intensity of the XPS signal given by [52,57,58]

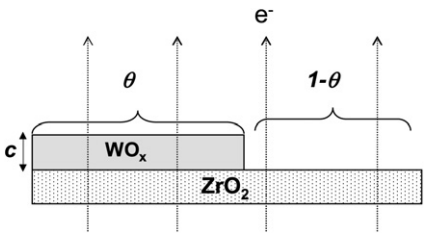

Fig. 5. Schematic representation of the model used to simulate experimental XPS data. WZ samples are modeled as consisting of ZrO_2 particles having semi-infinite thickness overlaid by parallelepiped-shaped WO_x clusters having vertical dimension c. In the model, θ represents the fraction of support surface covered by the WO_x overlayer.

$$I = nf\sigma D\lambda, \tag{1}$$

where I is the intensity of the XPS peak, n is the number of atoms per cm^3 of the element of interest, f is the flux of X-ray photons impinging on the sample, σ is the photoelectric cross-section for the particular transition in cm^2 per atom, D is the detection efficient coefficient, and λ is the inelastic mean free path (IMFP), or attenuation length, of the photoelectrons in the sample. D depends on the kinetic energy of the electron according to the expression $(KE)^{-0.82}$. The photoelectric cross-sections (σ) are taken from Scofield's theoretical values [59], and the attenuation lengths (λ) are calculated as proposed by Seah [57].

In the present study, WZ solids were modeled as consisting of ZrO_2 particles with semi-infinite thickness and displaying parallelepiped-shaped WO_x overlaying clusters with vertical dimension c [60], as shown schematically in Fig. 5. Experimental XPS intensity values were corrected by a factor of 2, thus accounting for surface roughness and support morphology [60,61]. Normal emission to the macroscopic surface ($\alpha = 90°$) is assumed in our model.

Taking into account (1) and the applied model, detected XPS intensities for W and Zr were simulated according to

$$\frac{I_W}{I_Z} = \frac{D_W\sigma_W\lambda_W\rho_W(1 - e^{-c/\lambda_W})}{D_Z\sigma_Z\lambda_Z\rho_Z(1-\theta) + D_Z\sigma_Z\lambda_{ZW}\rho_Z\theta(e^{-c/\lambda_{ZW}})}. \tag{2}$$

In this equation, D_i and σ_i are the detection coefficients and the photoelectric cross-sections, respectively, for each i-atom (i = W, Zr), and ρ_W and ρ_Z account for the W and Zr atomic densities, respectively. λ_W represents the IMFP of the tungsten electrons in the supported tungsten overlayer, λ_{ZW} represents the IMFP of electrons from the ZrO_2 support through the supported tungsten phase, and λ_Z represents the IMFP of the zirconia photoelectrons. The parameter θ denotes the surface covered by the WO_x domains expressed as a fraction of the total surface. According to (2), tungsten intensity is due to photoelectrons coming from a WO_x slab overlaying the ZrO_2 support and having limited thickness, c. On the other hand, zirconium intensity is composed of two types of photoelectrons,

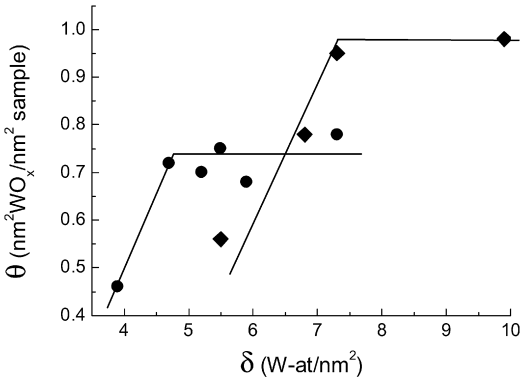

Fig. 6. Change of the XPS model parameter θ with the tungsten surface density (δ) for WZ samples prepared by impregnation (●) and coprecipitation (◆). Lines are guides for the viewer.

those coming from a noncovered ZrO_2 surface $(1-\theta)$ and those emitted from a ZrO_2 surface covered by the c-sized WO_x domains (θ). The term $e^{-c/\lambda_{ZW}}$ accounts for attenuation through the WO_x overlayer.

The experimental XPS intensity ratios were fitted for each WZ sample by adjusting c and θ. Only 1 degree of freedom was allowed because the parameters c and θ are interrelated according to

$$\theta = \frac{x}{A\rho_W c}, \tag{3}$$

where x is the tungsten content for each sample (g_W/g_{sample}), A is the BET total surface area, and ρ_W is the tungsten atomic density.

The values obtained for the c and θ parameters of the applied XPS model are given in Table 2. Keep in mind that these values must be considered only on a qualitative basis. Thus, the interdependent parameters c (accounting for vertical growth of tungsten species) and θ (fraction of surface covered by the WO_x domains) must be taken as representative average values for the locally heterogeneous surface of the WZ materials, although they are meaningful from a comparative standpoint. Fig. 6 depicts the mean coverage (θ) against the tungsten surface density (δ) for the impregnated and coprecipitated series. As observed, θ increases with increasing δ until a plateau is reached for both the impregnated and coprecipitated series.

Two main qualitative observations can be made based on the results in Fig. 6 derived from the XPS model applied. First, the inflexion in the θ–δ plot occurs at a higher value of δ for the coprecipitated catalysts, in agreement with the fact that in these samples, the growth of three-dimensional WO_3 crystallites occurs at a higher W surface density than in the impregnated series, as evidenced by XRD and Raman. Second, a higher mean coverage (θ) is attained for the coprecipitated samples at the plateau, suggesting a better capability to disperse the tungsten species on the ZrO_2 surface by this preparation route compared with impregnation. Such a high spreading capacity inherent to the coprecipitation method determines that the formation of highly interconnected WO_x domains, required for the generation of catalytically active acid sites, occurs at higher tungsten surface densities than in samples prepared by impregnation.

The differences between the two preparation methods observed from the modeled XPS results are also reflected in the distinct catalytic behavior reported here for the hydroconversion of n-hexadecane, that is, the greater W surface density required to attain the maximum catalytic activity (δ_{max}) and the less pronounced change in activity and selectivity on surpassing δ_{max} for the coprecipitated catalysts. Moreover, the more efficient use of the ZrO_2 surface achieved in WZ materials prepared by coprecipitation may explain their higher reaction rate by the unit surface area attained at $\delta = \delta_{max}$ compared with those obtained by impregnation (Fig. 1b). However, the intrinsic activity (TOF) at δ_{max} is almost the same for the two preparation methods (Fig. 1a), suggesting that large differences in the size of the amorphous WO_x domains, which are directly related to their ability to stabilize reduced centers and thus to the TOF [6], should not be expected for the most active samples within each series. This finding appears to conflict with the lower coverage ($\theta = 0.69$) obtained from the XPS model for the impregnated WZ(I,5.2) sample compared with WZ(C,6.8) prepared by coprecipitation ($\theta = 0.78$), but actually does not if the facts that the W content in both samples is similar (18–19 wt%) and that the former has a significantly larger BET surface area (120 against 87 m^2/g) due to the lower annealing temperature applied during its activation are taken into account. Then, combining the characterization with the catalytic data discussed up to now, we can conclude that the coprecipitation method allows better utilization of the ZrO_2 surface for generation of WO_x domains above the minimum critical size required for the development of catalytically active sites. Consequently, the generation of those WO_x domains and the growth of catalytically inactive WO_3 crystallites occur at higher tungsten surface densities in samples prepared by coprecipitation than in those obtained by impregnation, leading to the observed shift in δ_{max} ($\delta_{max,COP} > \delta_{max,IMP}$).

The reduction behavior of the supported tungsten phases in WZ catalysts was studied by H_2-TPR. Pt-loaded WZ samples were used for the H_2-TPR measurements to locate the reduction features within the temperature range covered by the experiment (room temperature to 1173 K), even for the less reducible samples. Fig. 7 shows the reduction profiles for the impregnated and coprecipitated Pt/WZ catalysts in the temperature range in which features due to tungsten reductions appear ($T > 500$ K). As observed, the most important onset for the H_2 consumption in both series occurs above 800 K, which, according to Refs. [2,5,6,62], is ascribed to the total reduction of supported tungsten species ($W^{6+} \rightarrow W^0$). Moreover, the total H_2 consumption rises, and the maximum shifts toward lower temperatures with increased tungsten surface density, in agreement with previous observations [5,6]. These findings indicate that larger and more interconnected WO_x clusters formed at increasing δ are easier to reduce than smaller and more isolated ones prevailing at low W surface densities regardless of the preparation method used. Moreover, for samples displaying comparable intrinsic catalytic activity (TOF) within the two series, those prepared by coprecipitation show slightly higher reducibilities for the amorphous WO_x clusters, as deduced from their lower temperatures of maximum H_2 consumption (T_{max}) in the corresponding

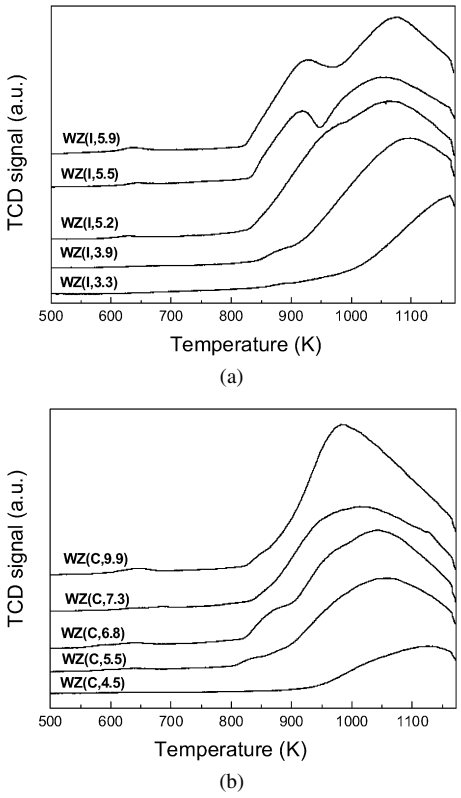

Fig. 7. H_2-TPR profiles for Pt/WZ catalysts prepared by (a) impregnation and (b) coprecipitation in the temperature range where tungsten reduction features appear ($T > 500$ K).

H_2-TPR profiles. Such a comparison based on TOF values is more appropriate than one based on δ because, as discussed earlier, the coprecipitation route introduces a delay in attaining a certain degree of interconnectivity of the WO_x domains with increasing δ with respect to the impregnation method. For instance, for the most active catalysts within each series displaying quite similar turnover rates (Fig. 1a), T_{max} reaches 1062 K for the impregnated sample and 1039 K for the coprecipitated sample, indicating the higher reducibility of the latter.

Along with the main reduction feature observed in the 1050–1200 K temperature range associated with the reduction of supported amorphous WO_x domains [31], an additional reduction peak at ca. 920 K develops for the impregnated samples at W surface densities above 5.2 W at/nm^2 (Fig. 7a), that is, above the density for which maximum catalytic activity is attained ($\delta_{max,IMP}$). This feature is ascribed to the reduction of tungsten in WO_3 crystallites existing on the ZrO_2 surface and detected by XRD and Raman. The increased relative intensity for this peak with respect to that ascribed to the amorphous WO_x phase for sample WZ(I,5.9) is in line with its assignment to WO_3 reduction. In contrast, the WO_3 reduction feature is not clearly distinguished for the coprecipitated catalysts (Fig. 7b), even for W surface densities above $\delta_{max,COP}$ (6.8 W at/nm^2). This is most likely related to a smaller crystallite size of the three-dimensional WO_3 species developing on the ZrO_2 surface at $\delta > \delta_{max}$ when the catalysts are prepared by coprecipitation instead of impregnation. In fact, decreased reducibility of WO_3 species with decreasing crystallite size already has been reported by Vaudagna et al. [2]. These authors attributed this effect to a stronger interaction of WO_3 crystallites with the support, which can be expected for coprecipitated samples in our case. This interpretation also agrees with the XRD characterization results, which showed weaker and broader diffractions for WO_3 crystallites in the coprecipitation series at high δ values (Fig. 3b). Although a strong band of WO_3 species was observed in the Raman spectrum of the coprecipitated WZ(C,9.9) sample (Fig. 4b), note that Raman spectroscopy allows the detection of very small WO_3 crystallites due to the high scattering cross-section for discrete WO_3 particles compared with surface species; thus, it is not an appropriate technique for establishing differences in crystallite size.

The catalytic and the structural characterization results discussed above indicate some significant differences between the impregnation and coprecipitation preparation routes. Despite such differences, however, it seems that a similar nature of the active WO_x species and thus an analogous catalytic performance can be attained by both methods, provided that the catalysts are compared at the appropriate W surface density. Nonetheless, intuitively, one might expect some differences in the electronic properties of the WO_3 clusters arising from differing interactions of those species with the zirconia support when generated by impregnating a presynthesized zirconia oxohydroxide or by activating an originally mixed W–Zr hydroxide. To prove this hypothesis, we used diffuse-reflectance UV–vis spectroscopy, a powerful characterization technique for studying electronic properties in WZ materials [6,23,47]. In the next section we discuss the DRS UV–vis results obtained for selected samples prepared by impregnation and coprecipitation methods, as well as for WO_3 used as reference.

3.4. Properties of WO_x species studied by diffuse-reflectance UV–vis spectroscopy

3.4.1. Analysis of the absorption edge energy in oxidized WZ samples

Figs. 8a and 8b collect the DR UV–vis spectra for the calcined samples synthesized by impregnation and polymer-templated coprecipitation, respectively. All of the WZ catalysts display main absorption features at energies ranging from 3.5 to 2.6 eV due to ligand-to-metal charge transfers in tungsten species existing on the ZrO_2 surface [47]. We discuss the results on the basis of the optical absorption edge energy (AEE) rather than on the position of bands, which are typically very broad, because the former allows a more rigorous measurement at the incipient absorption region. The AEE values were obtained by using the model typically applied for indirect-allowed HOMO-LUMO transitions occurring in amorphous nanosized semiconductor domains, which have been successfully used to characterize WO_x species supported on metallic oxides [47,63]. Thus, the AEE values were determined by finding the x-intercept of the straight tangent line at the proximity of the absorption onset in the $(F(R)h\nu)^{1/\eta}$ versus $h\nu$ plots, where $F(R)$ is the Kubelka function, $h\nu$ is the incident photon energy, and $\eta = 2$ for indirect-allowed transitions [64]. The AEE values thus obtained are plotted in Fig. 9 against the tungsten surface density (δ) for

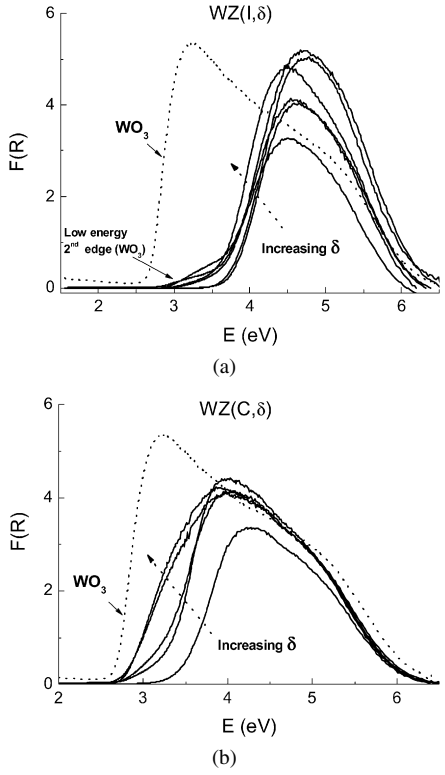

Fig. 8. Diffuse reflectance UV–vis absorption spectra for (a) impregnated and (b) coprecipitated WZ samples with different tungsten surface densities. The spectrum of the reference bulk WO_3 solid (dotted line) is also included for comparison. $F(R)$ is the Kubelka–Munk function and E is the photon energy.

both series of WZ samples. To clarify the discussion of the UV–vis results, the qualitative change in the intrinsic activity (TOF) with δ for the impregnated and coprecipitated samples is also included (dashed and dotted lines, respectively). As observed, the AEE initially decreases with increasing δ for both series of catalysts. This trend, which was previously found for WZ catalysts prepared by impregnation [47,63] and, as shown here, also applies to coprecipitation methods, is ascribed to an increase in the size of the supported WO_x domains with increasing W surface density. Besides this general trend, significant differences between the two preparation methods arose from the analysis of the AEE data, as discussed below.

Fig. 9 shows that the AEE for the impregnated samples declines from ca. 3.5 to ca. 3.2 eV with increasing δ from 3.3 to 5.2 W at/nm^2 (corresponding to the density of maximum catalytic activity, $\delta_{max,IMP}$) and then remains constant at higher values of δ, suggesting no further increase in the size of the amorphous polytungstate domains at W surface densities above $\delta_{max,IMP}$. Furthermore, impregnated WZ samples with $\delta > \delta_{max,IMP}$ display an additional low-energy AEE associated with WO_3 clusters, as reported by Iglesia et al. [47]. The slightly higher AEE displayed by the WO_3 clusters existing in WZ samples compared with that of WO_3 (crystal size ca. 38 nm as determined by XRD) is likely due to a broadening of the conduction-valence energy gap caused by a quantum size effect, in line with their much smaller crystal size [65]. In contrast, in the coprecipitated samples, the AEE asymptotically approaches 2.59 eV (which is the AEE for bulk WO_3)

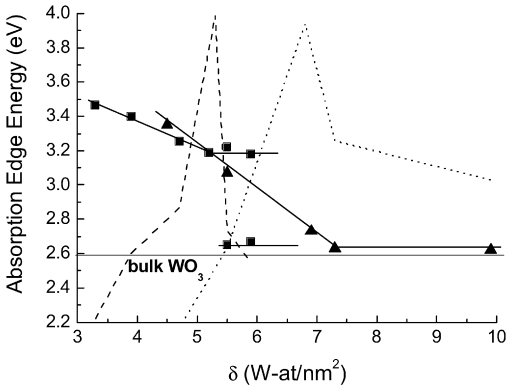

Fig. 9. Absorption edge energies (AEE) as a function of the tungsten surface density (δ) in WZ samples prepared by impregnation (■) and coprecipitation (▲) methods. The AEE obtained for bulk WO_3 is also shown for comparison. The qualitative change of TOF with δ for the impregnated and coprecipitated Pt/WZ catalysts has been included as dashed and dotted lines, respectively.

without splitting into two AEE values even for samples with W surface densities well above $\delta_{max,COP}$ (6.8 W at/nm^2). This suggests that the development of WO_3 crystallites on the ZrO_2 surface at high W densities occurs differently for the two preparation methods. In the case of impregnation, the relatively weak interaction of the supported tungsten species with the zirconia surface leads to larger WO_3 crystallites at $\delta > \delta_{max}$ (as deduced from XRD and H_2-TPR), which are electronically isolated from the support and the coexisting amorphous WO_x phase, resulting in the splitting of the AEE signal at $\delta > \delta_{max,IMP}$ (Fig. 9).

Regarding the WZ(C,7.3) sample prepared by coprecipitation with a W surface density slightly exceeding $\delta_{max,COP}$, XRD, Raman, and H_2-TPR results suggest the presence of minor amounts of WO_3 crystallites on the surface coexisting with the predominant amorphous WO_x phase. However, the AEE value for this sample is close to that of WO_3 (Fig. 9). Taking into account the sensitivity of AEE values (in the range 3.54–2.59 eV) to subtle changes in the cluster packing for different tungsten species with octahedrally coordinated W atoms [48], it cannot be ruled out that the AEE value for this sample also may be characteristic of highly polymerized amorphous WO_x clusters with a structure closely resembling that of crystalline WO_3 through enhanced corner-sharing for the neighboring W-octahedra [48]. In this case, the expected stronger interaction of W species with the zirconia support in coprecipitated samples likely retards the transition toward well-developed WO_3 crystallites up to higher coverages in comparison with impregnated solids.

It is also interesting to note that in Fig. 9, the coprecipitated samples display lower AEE than the impregnated counterparts within almost the entire range of δ. A direct relationship between AEE and polytungstate domain size has been established for homogeneous series of WZ catalysts prepared by impregnation [47,63,66]. Nevertheless, catalysis also provides indirect evidence for the WO_x domain size in samples with tungsten surface densities below δ_{max}, because it is known that larger WO_x domains reduce more easily and allow stabilization of a larger number of strong acidic sites by electron delocalization [6,47]. Taking this into account, differences in the polytungstate

domain size cannot account for the distinct AEE values obtained for the two series of samples, because the two catalysts exhibiting maximum catalytic activity within each series [WZ(I,5.2) and WZ(C,6.8)] have similar TOFs (and thus similar WO_x domain sizes) but quite different AEE values. Thus, it is pertinent to hypothesize here that reasons other than WO_x domain size must be behind the generally lower AEE displayed by coprecipitated samples.

It is known that not only the size of amorphous metal oxide domains, but also the nature of the oxidic carrier on which they are deposited, determine the valence–conduction energy gap for the bulk solid and thus its behavior in photoexcited phenomena. In this respect, WO_x domains supported on more isolating carriers, such as Al_2O_3, display higher UV-AEE than those supported on TiO_2 or ZrO_2 [47,67]. Obviously, no effects due to the nature of the support may be expected in our samples, because t-ZrO_2 is the common carrier for both the impregnated and coprecipitated samples with the exception of sample WZ(C,4.5), as discussed earlier. In addition, crystallite size is also known to affect the electronic properties of pure and mixed oxides displaying very small crystal size (<10 nm) due to quantum size effects [68–70]. However, in our case, even if the two preparation methods lead to slightly different t-ZrO_2 crystal sizes in the final WZ samples (7–8 nm for coprecipitated and 8–10 nm for impregnated), the coprecipitated solids are those displaying a lower AEE, whereas the opposite trend should be expected on the basis of an hypothetical quantum size effect, which produces a blue-shift instead of a red-shift in the conduction-valence band-gap energy with decreasing oxide crystal size. Unfortunately, very little information is available in the literature regarding the influence of preparation route on the electronic properties of supported amorphous metal oxide domains. In this respect, Weber [71] attempted to rationalize this effect for silica-supported MoO_x species on the basis of UV-AEE data. Interestingly, he found that samples prepared by a grafting route displayed lower AEE values than those prepared by impregnation within a wide range of molybdenum surface densities [71]. Thus, it was suggested that the method of incorporating the molybdenum species altered the electronic properties of the supported oxide clusters, although some slight differences in domain size were not overlooked. On the other hand, the influence of surface (i.e., impregnation) and bulk (i.e., coprecipitation) metal doping on the optical, photochemical, and electronic properties for some metal oxides has been studied [67,72–75]. It was found that surface doping of TiO_2 with WO_x did not modify the UV-AEE compared with pure anatase, because the $O^{2-} \rightarrow W^{6+}$ and $O^{2-} \rightarrow Ti^{4+}$ charge transfers overlap (W5d orbitals energy lie within the Ti3d conduction band) [67], but, interestingly, WO_x–TiO_2 samples obtained by coprecipitation displayed a red-shift in the valence–conduction band-gap energy compared with those obtained by surface doping with similar W loadings [75]. Anion vacancies created by substitutional doping involving Ti^{IV} and W^{VI} atoms, also proposed in similar systems such as MoO_x–TiO_2 and NbO_x–TiO_2 [75], were seen to be responsible for the decreased UV-AEE, although no detailed physical explanation for this has been yet put forward.

Taking this finding and our UV–vis results discussed earlier into account, we may hypothesize that the differences in AEE values observed for WZ samples prepared by impregnation and coprecipitation might be related to a different electronic interaction between the surface tungsten species and zirconia. Thus, although both preparative routes are capable of stabilizing the t-ZrO_2 phase on high-temperature oxidation treatment and developing active surface WO_x species, their optical and electronic properties are determined by the synthesis procedure. Even if WO_x species are located on the surface of zirconia for both methods, as confirmed by XPS, some substitutional intergrowth between t-ZrO_2 and WO_x may occur at the interface in coprecipitated samples, leading to the formation of anion vacancies responsible for the observed red-shift in AEE values compared with the impregnated ones.

3.4.2. Reduction kinetics of supported WO_x domains monitored by in situ DRS UV–vis

It is now widely accepted that temporary acidic sites develop on WZ catalysts on exposure to reductants, such as H_2, alkanes, or alcohols, leading to the formation of partially reduced $W^{(6-\delta)+}$ centers from the initial W^{VI} species [6,47,51]. Thus, the strength of the formed acidic sites depends on the capability of the amorphous polytungstate domains to effectively delocalize the electron density [76]. DR UV–vis spectroscopy has proven to be a valuable technique for characterizing supported polytunsgtate species because delocalization of the negative charge, together with the appearance of metallic d–d transitions in reduced W^{5+} centers, leads to the appearance of absorption features in the visible region on exposure of WZ samples to reductants [6,47,77]. Iglesia et al. [23,47,63] have demonstrated that useful information on the kinetics of reduction and the formation of reduced $W^{(6-\delta)+}$ centers, which are directly linked to the development of strong Brønsted acidity in WZ solids, can be obtained by integrating the visible absorption in the pre-edge region of the UV–vis spectra. When we did this for our two series of WZ samples, we found (results not shown) that the integrated pre-edge absorption in Pt-promoted WZ samples previously submitted to the same reduction treatment applied before catalysis (reduction under flowing H_2 at 523 K for 2 h) increased with increasing tungsten surface density (δ) irrespective of the preparation method used. This general feature is in line with the expected increase in the amount of reduced tungsten centers with increasing size of the supported WO_x domains [23,47]. These results are also congruent with those obtained by DRIFTS of adsorbed acetonitrile on reduced WZ samples prepared by coprecipitation addressed in a recent work from our group [12], which indicated an increased strength of temporary Brønsted acid sites with increasing δ up to the density of maximum activity $\delta_{max,COP}$. In our in situ reduction DRS UV–vis study, we still observed increased visible absorption at tungsten densities above δ_{max} in the two series of samples, ascribed to the known capacity of crystalline WO_3 species to generate colored bronzes on reduction [78] despite their known inactivity in catalysis.

In this study, we found that at the tungsten surface density of maximum catalytic activity (δ_{max}), the sample prepared by

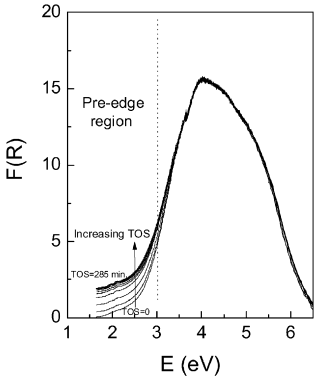

Fig. 10. DR UV–vis spectra of sample WZ(C,6.8) obtained at different times (TOS) during in situ reduction treatment at 523 K in flowing H_2. Note that only the intensity of the absorption in the pre-edge (visible) region increases with TOS until a stationary state is attained.

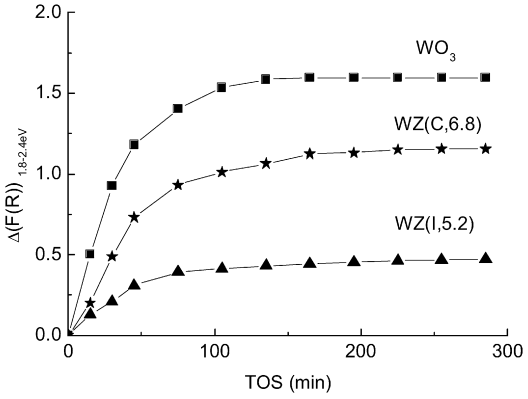

Fig. 11. Integrated absorption change of the pre-edge UV–vis region during in situ reduction at 523 K as a function of TOS for WO_3 (reference) and WZ samples displaying maximum catalytic activity ($\delta = \delta_{max}$) within the impregnated (WZ(I,5.2)) and coprecipitated (WZ(C,6.8)) series.

coprecipitation displayed a lower AEE than that prepared by impregnation, despite a similar WO_x domain size may be expected for both catalysts on the basis of their comparable TOF. Moreover, at comparable TOF, WO_x species in the coprecipitated samples were slightly more reducible than those in the impregnated samples. These results concur with the general trends reported for oxide-supported oxometallic (MO_x) species showing that a lower energy gap between the valence and conduction bands increases the reducibility of the supported oxides [66,79]. We also studied the reduction kinetics of the two samples with $\delta = \delta_{max}$ using in situ DR UV–vis spectroscopy under flowing H_2 at 523 K (see Section 2). We performed the study on the Pt-free samples to avoid the possible interference of hydrogen spillover phenomena that may occur on the Pt sites and can mask true reduction kinetics for the supported tungsten species. In fact, it has been shown that a certain reduction of tungsten in Pt/WZ catalysts readily occurs under H_2 flow even at room temperature [39]. Our in situ reduction UV–vis study used an energy range 1.8–2.4 eV as representative of the pre-edge adsorption region to register the integrated changes of the Kubelka–Munk function with time on stream (TOS), as previously proposed by Barton et al. [47]. Fig. 10 shows a representative plot of the evolution of the pre-edge absorption region in the UV–vis spectra with TOS for the coprecipitated WZ(C,6.8) sample. As can be seen, no appreciable changes in the postedge region (photon energies >3.5 eV) occurs, in line with previous observations [47]. In contrast, a gradual increase in the pre-edge absorption can be seen up to a certain TOS, after which no further changes in the UV–vis spectra occur. The results in Fig. 10 clearly show that the rate of change in pre-edge absorption decreases with TOS until it becomes nearly zero in the stationary state. A broad band at ca. 2.19 eV, ascribed to *d–d* electronic transitions in the formed reduced W^{5+} sites, is also seen. Similar trends were found for the impregnated WZ(I,5.2) sample (not shown). Fig. 11 reflects the integrated absorption changes in the pre-edge region against TOS for the two samples with $\delta = \delta_{max}$ within the two series, as well as for bulk WO_3 used as reference. As observed, the initial reduction rate is highest for WO_3, which is known to undergo slight reductions more readily than amorphous WO_x species [47]. Interestingly, the initial reduction rate was significantly higher for WZ(C,6.8) than for the impregnated WZ(I,5.2) counterpart, thus confirming that the lower AEE observed in the former provides an enhanced surface reduction of the supported WO_x domains. It is worth recalling here that the observed differences in reduction kinetics are intrinsic to the preparation method; comparable WO_x domain sizes may be expected for the two samples displaying nearly the same TOF.

It should be mentioned at this point that the differences in the WO_x reduction kinetics inherent to the preparation method used can be expected to diminish or even vanish in the Pt-promoted catalysts subjected to the 2-h reduction treatment at 523 K in flowing H_2, due to the assistance of the metal sites in activating hydrogen. Thus, this effect will have little or no influence during catalysis. Moreover, the pre-edge absorption attained in the steady state of the in situ reduction process was found to be greater for the coprecipitated sample, again pointing out the greater reducibility of the WO_x domains in the coprecipitated sample compared with its impregnated counterpart. It also should be mentioned that because the two analyzed WZ(I,5.2) and WZ(C,6.8) samples have similar W content (19 and 18 wt%, respectively; see Table 1), the distinct steady-state absorptions cannot be ascribed to different W loadings; in the case of bulk WO_3, the absence of dilution by ZrO_2 is likely responsible for its higher absorption.

4. Conclusion

In this study, two series of high-surface area tungstated zirconia (WZ) samples comprising a wide range of tungsten surface densities (δ, W at/nm^2) were prepared by modified impregnation and coprecipitation methods, followed by annealing at 973–1073 K. The two series of Pt-promoted WZ catalysts (1 wt% Pt) showed characteristic patterns in activity and selectivity during the hydroconversion of *n*-hexadecane as a function of δ. Thus, a maximum in the catalytic activity and a minimum in the selectivity to branched feed isomers (at constant conversion) were attained at an intermediate tungsten surface density (δ_{max}). Despite the fact that both series of catalysts displayed the same general trends in activity/selectivity with increasing δ,

the catalysts prepared by the coprecipitation route required a higher tungsten surface density to attain the maximum catalytic activity ($\delta_{max,COP} = 6.8$ W at/nm^2) compared with those obtained by impregnation ($\delta_{max,IMP} = 5.2$ W at/nm^2), even though both methods led to catalysts with nearly the same TOF at their respective δ_{max}. Moreover, the change in activity and selectivity at δ above the respective δ_{max} was much less pronounced for coprecipitated catalysts. These differences can be explained by the lower tendency toward sintering of the surface WO_x species on high-temperature annealing treatment when generated by migration from the bulk of a coprecipitated W–Zr solid to the zirconia surface instead of by titrating the surface Zr–OH groups through impregnation with the tungsten precursor. This indicates that a higher W surface density is required in coprecipitated catalysts to produce the highly interconnected amorphous WO_x domains needed for the generation of catalytically active Brønsted acid sites on reduction and to retard the onset of growth of three-dimensional WO_3 crystallites on the ZrO_2 surface.

Our findings allow the reconciliation of discrepancies found in the literature concerning the influence of preparation method on the structural and catalytic properties of WZ solid acids. Besides the aforementioned structural and catalytic differences, the preparation method also affects the optical and electronic properties of the supported WO_x domains. The polytungstate clusters in WZ samples prepared by coprecipitation are characterized by a lower UV–vis absorption edge energy (i.e., lower valence–conduction energy gap for the WZ solids) and enhanced reducibility compared with those generated by impregnation, probably due to enhanced formation of anion vacancies by substitutional intergrowth at the interface between t-ZrO_2 and WO_x species.

Acknowledgments

Financial support by the Comisión Interministerial de Ciencia y Tecnología (CICYT) of Spain through project CTQ2004-02510/PPQ is gratefully acknowledged. G. Prieto thanks the Ministerio de Educación y Ciencia (MEC) of Spain for a doctoral scholarship.

References

[1] J.G. Santiesteban, D.C. Calabro, W.S. Borghard, C.D. Chang, J.C. Vartuli, Y.P. Tsao, M.A. Natal-Santiago, R.D. Bastian, J. Catal. 183 (1999) 314.
[2] S.R. Vaudagna, R.A. Comelli, N.S. Fígoli, Appl. Catal. A 164 (1997) 265.
[3] M.A. Arribas, F. Márquez, A. Martínez, J. Catal. 190 (2000) 309.
[4] S. Kuba, P. Lukinskas, R. Ahmad, F.C. Jentoft, R.K. Grasselli, B.C. Gates, H. Knözinger, J. Catal. 219 (2003) 376.
[5] E. Iglesia, D.G. Barton, S.L. Soled, S. Miseo, J.E. Baumgartner, W.E. Gates, G.A. Fuentes, G.D. Meitzner, Stud. Surf. Sci. Catal. 101 (1996) 533.
[6] D.G. Barton, S.L. Soled, G.D. Meitzner, G.A. Fuentes, E. Iglesia, J. Catal. 181 (1999) 57.
[7] T.N. Vu, J. van Gestel, J.P. Gilson, C. Collet, J.P. Dath, J.C. Duchet, J. Catal. 231 (2005) 468.
[8] S.G. Zhang, Y.L. Zhang, J.W. Tierney, I. Wender, Appl. Catal. A 193 (2000) 155.
[9] J. Walendziewski, B. Pniak, B. Malinowska, Chem. Eng. J. 95 (2003) 113.
[10] S.G. Zhang, Y.L. Zhang, J.W. Tierney, I. Wender, Fuel Process. Technol. 69 (2001) 59.
[11] C.D. Chang, S. Han, D.J. Martenak, J.G. Santiesteban, D.E. Walsh, US Patent 6,217,747 (2001), assigned to Mobil Oil Corp.
[12] A. Martínez, G. Prieto, M.A. Arribas, P. Concepción, Appl. Catal. A 309 (2006) 224.
[13] S.T. Sie, M.M. Senden, H.M.H. van Wechem, Catal. Today 8 (1991) 371.
[14] M.E. Dry, Appl. Catal. A 189 (1999) 185.
[15] G. Larsen, E. Lotero, R.D. Parra, L.M. Petkovic, H.S. Silva, S. Raghavan, Appl. Catal. A 130 (1995) 213.
[16] F.T.T. Ng, N. Horvat, Appl. Catal. A 123 (1995) 197.
[17] G. Larsen, E. Lotero, R.D. Parra, in: Proc. 11th Intl. Congr. Catal., Baltimore, 1996, p. 543.
[18] R.A. Boyse, E.I. Ko, J. Catal. 171 (1997) 191.
[19] D.G. Barton, S.L. Soled, E. Iglesia, Topics Catal. 6 (1998) 87.
[20] F. Figueras, J. Palomeque, S. Loridant, C. Fèche, N. Essayem, G. Gelbard, J. Catal. 226 (2004) 25.
[21] M. Valigi, D. Gazzoli, I. Pettiti, G. Mattei, S. Colonna, S. De Rossi, G. Ferraris, Appl. Catal. A 231 (2002) 159.
[22] M. Scheithauer, T.K. Cheung, R.E. Jentoft, R.K. Grasselli, B.C. Gates, H. Knözinger, J. Catal. 180 (1998) 1.
[23] C.D. Baertsch, K.T. Komala, Y.-H. Chua, E. Iglesia, J. Catal. 205 (2002) 44.
[24] M. Scheithauer, R.K. Grasselli, H. Knözinger, Langmuir 14 (1998) 3019.
[25] T.N. Vu, J. van Gestel, J.P. Gilson, C. Collet, J.P. Dath, J.C. Duchet, J. Catal. 231 (2005) 453.
[26] R.D. Wilson, D.G. Barton, C.D. Baertsch, E. Iglesia, J. Catal. 194 (2000) 175.
[27] D.S. Kim, M. Ostromecki, I.E. Wachs, J. Mol. Catal. A 106 (1996) 93.
[28] F. Di Gregorio, V. Keller, J. Catal. 225 (2004) 45.
[29] M.G. Falco, S.A. Canavese, N.S. Fígoli, Catal. Today 107–108 (2005) 778.
[30] J.G. Santiesteban, J.C. Vartuli, S. Han, R.D. Bastian, C.D. Chang, J. Catal. 168 (1997) 431.
[31] D.C. Calabro, J.C. Vartuli, J.G. Santiesteban, Topics Catal. 18 (2002) 231.
[32] M.A. Cortés-Jácome, J.A. Toledo, C. Angeles-Chavez, M. Aguilar, J.A. Wang, J. Phys. Chem. B 109 (2005) 22730.
[33] A. Barrera, J.A. Montoya, M. Viniegra, J. Navarrete, G. Espinosa, A. Vargas, P. del Angel, G. Pérez, Appl. Catal. A 290 (2005) 97.
[34] F.G.R. Gimblett, A.A. Rahman, K.S.W. Sing, J. Colloid Interface Sci. 84 (1981) 337.
[35] O.V. Melezhyk, S.V. Prudius, V.V. Brei, Micropor. Mesopor. Mater. 49 (2001) 39.
[36] P.B. Weisz, in: D.D. Eley, P.W. Selwood, P.B. Weisz (Eds.), in: Advances in Catalysis and Related Subjects, vol. 13, Academic Press, New York, 1962, p. 137.
[37] J.G. Santiesteban, D.C. Calabro, C.D. Chang, J.C. Vartuli, T.J. Fiebig, R.D. Bastian, J. Catal. 202 (2001) 25.
[38] J.C. Yori, C.R. Vera, J.M. Parera, Appl. Catal. A Gen. 163 (1997) 165.
[39] S. Kuba, P. Lukinskas, R.K. Grasselli, B.C. Gates, H. Knözinger, J. Catal. 216 (2003) 353.
[40] S. Kuba, P.C. Heydorn, R.K. Grasselli, B.C. Gates, M. Che, H. Knözinger, Phys. Chem. Chem. Phys. 3 (2001) 146.
[41] S.V. Filimonova, A.V. Nosov, M. Scheithauer, H. Knözinger, J. Catal. 198 (2001) 89.
[42] A.G. Pelmenschikov, R.A. van Santen, J. Jänchen, E. Meijer, J. Phys. Chem. 97 (1993) 11071.
[43] O. Cairon, T. Chevreau, J.C. Lavalley, J. Chem. Soc. Faraday Trans. 94 (1998) 3039.
[44] K. Shimizu, T.N. Venkatraman, W. Song, Appl. Catal. A 225 (2002) 33.
[45] G. Larsen, L.M. Petkovic, Appl. Catal. A 148 (1996) 155.
[46] L.M. Petkovic, J.R. Bielenberg, G. Larsen, J. Catal. 178 (1998) 533.
[47] D.G. Barton, M. Shtein, R.D. Wilson, S.L. Soled, E. Iglesia, J. Phys. Chem. B 103 (1999) 630.
[48] D.L. Poster, J. Am. Ceram. Soc. 62 (1979) 298.
[49] S.S. Chan, I.E. Wachs, L.L. Murrell, N.C. Dispenziere Jr., J. Catal. 92 (1985) 1.
[50] S.R. Vaudagna, S.A. Cavanese, R.A. Comelli, N.S. Fígoli, Appl. Catal. A 168 (1998) 93.

[51] J.R. Sohn, M.Y. Park, Langmuir 14 (1998) 6140.
[52] C.D. Wagner, L.E. Davis, M.V. Zeller, J.A. Taylor, R.H. Raymond, L.H. Gale, Surf. Interface Anal. 3 (1981) 211.
[53] S.C. Fung, J. Catal. 58 (1979) 454.
[54] S.C. Fadley, R.J. Baird, W. Siekhaus, T. Novakov, S.A.L. Bergstrom, J. Electron Spectrosc. Relat. Phenom. 4 (1974) 93.
[55] V. Leon, Surface Sci. 339 (1995) L931.
[56] F.P.J.M. Kerkhof, J.A. Moulijn, J. Phys. Chem. 83 (1979) 1612.
[57] M.P. Seah, Surf. Interface Anal. 2 (1980) 222.
[58] T.A. Carlson, Surf. Interface Anal. 4 (1982) 125.
[59] H. Scofield, J. Electron Spectrosc. Relat. Phenom. 8 (1976) 129.
[60] A. Cimino, D. Gazzoli, M. Valigi, J. Electron Spectrosc. Relat. Phenom. 104 (1999) 1.
[61] A. Cimino, D. Gazzoli, M. Valigi, J. Electron Spectrosc. Relat. Phenom. 67 (1994) 429.
[62] A. Gutiérrez-Alejandre, P. Castillo, J. Ramírez, G. Ramis, G. Busca, Appl. Catal. A 216 (2001) 181.
[63] J. Macht, C.D. Baertsch, M. May-Lozano, S.L. Soled, Y. Wang, E. Iglesia, J. Catal. 227 (2004) 479.
[64] J. Tauc, Amorphous and Liquid Semiconductors, Plenum, Cambridge, 1978.
[65] L.G. Teoh, J. Shieh, W.H. Lai, I.M. Hung, M.H. Hon, J. Alloys Comp. 396 (2005) 251.
[66] K.D. Chen, A.T. Bell, E. Iglesia, J. Catal. 209 (2002) 35.
[67] A. Gutiérrez-Alejandre, J. Ramírez, G. Busca, Catal. Lett. 56 (1998) 29.
[68] I. Moriguchi, H. Maeda, Y. Teraoka, S. Kagawa, J. Am. Chem. Soc. 117 (1995) 1139.
[69] Y.-W. Zhang, R. Si, C.-S. Liao, C.-H. Yan, C.-X. Xiao, Y. Kou, J. Phys. Chem. B 107 (2003) 10159.
[70] F.X. Liu, X.Y. Zhang, Q. Wu, L. Liu, J.Y. Wang, Q.D. Su, J. Appl. Phys. 85 (2) (1999) 734.
[71] R.S. Weber, J. Catal. 151 (1995) 470.
[72] A.-W. Xu, Y. Gao, H.-Q. Liu, J. Catal. 207 (2002) 151.
[73] F.R. Sensato, R. Custodio, E. Longo, A. Beltrán, J. Andrés, Catal. Today 85 (2003) 145.
[74] A. Fuerte, M.D. Hernández-Alonso, A. Iglesias-Juez, A. Martínez-Arias, J.C. Conesa, J. Soria, M. Fernández-García, Phys. Chem. Chem. Phys. 5 (2003) 2913.
[75] M. Fernández-García, A. Martínez-Arias, A. Fuerte, J.C. Conesa, J. Phys. Chem. B 109 (2005) 6075.
[76] J.E. Herrera, J.H. Kwak, J.Z. Hu, Y. Wang, C.H.F. Peden, J. Macht, E. Iglesia, J. Catal. 239 (2006) 200.
[77] S. Kuba, M. Che, R.K. Grasselli, H. Knözinger, J. Phys. Chem. B 107 (2003) 3459.
[78] J.E. Benson, H.W. Kohn, M. Boudart, J. Catal. 5 (1966) 307.
[79] B. Samaranch, P. Ramírez de la Piscina, G. Clet, M. Houalla, N. Homs, Chem. Mater. 18 (2006) 1581.